# A plasmonic nanoledge array sensor for detection of anti-insulin antibodies of type 1 diabetes biomarker

By: Bhawna Bagra, Taylor Mabe, Frank Tukur, and Jianjun Wei

B. Bagra, T. Mabe, F. Tukur, J. Wei, A plasmonic nanoledge array sensor for detection of anti-insulin antibody of type 1 diabetes biomarker, *Nanotechnology*, **2020**, 31(32), DOI: 10.1088/1361-6528/ab8c05.



## Abstract:

Here we present a plasmonic nanoledge device with high sensitivity and selectivity used to detect protein biomarkers simply by functionalizing the device, which specifically binds to particular biomolecule or biomarkers. We employ this plasmonic nanoledge device for the detection of anti-insulin antibodies of type 1 diabetes (T1D) in buffer and human serum at the range of pg $ml^{-1}$ to 100 ng $ml^{-1}$. The signal transduction is based on the extraordinary optical transmission (EOT) through the nanoledge array and the optical spectral changes with the biological binding reaction between the surface functionalized insulin with anti-insulin antibody. Control experiments indicate little interferences from the human serum background and addition of other proteins such as bovine serum albumin (BSA) and epidermal growth factor (EGF) at 20 ng $ml^{-1}$. The high sensitivity, specificity and easy adaptability of the plasmonic device offer new opportunities in biosensing and diagnostic applications for T1D.

**Keywords:** nanoplasmonics | biosensor | anti-insulin antibody | biomarkers | type 1 diabetes

## Article:

### 1. Introduction

Biomolecules or biomarkers play an important role in disease diagnosis and treatment [1]. A few methods have been demonstrated for biomolecules or biomarker detection, including surface enhanced raman spectroscopy (SERS) [2], enzyme-linked immunosorbent assay (ELISA) [3], colorimetry [4], and electrochemical assay [5]. There are unmet needs which motivate to improve performance in terms of sensitivity, detection limit, turnaround time, sample amount, sample preparation requirements, multiplexing (multiple samples at a time), instrumentation, compactness, and portability [1]. The use of metal nanostructures in the biosensors has been attractive and one of the most promising alternative methods [6]. Noble metal nanostructures have the property of surface plasmon resonance (SPR) [7], this property can be utilized to improve the sensitivity and selectivity of the currently available methods [8].

SPR detection methods have been gaining popularity lately because of their ability to handle complex samples and to provide label-free optical biosensors with real time detection [8–10]. These sensors can handle complex samples such as human serum/blood without tedious preparation and pretreatment [11, 12]. SPR makes use of nanostructures and/or nanostructured metal films which remove the need for complex detection instrumentation [13]. These abilities of SPR make it a good candidate for creating a plasmonic sensor which is easy to use, reliable, capable of on-site detection, selective, and sensitive enough to measure low concentration of biomolecules or biomarker targets [14–17]. Coupled with microfluidics, SPR detection can be used as a handheld device for easy diagnosis and treatment [18].

SPR can present localized surface plasmon resonance (LSPR) or surface plasmon polariton (SPP) [19], which can increase the local field near the metallic surfaces for sensing, optical enhancement, and/or energy conversion [20–24]. When the metal structure gets smaller than the wavelength of incident light, it gives rise to a phenomenon called LSPR. LSPR is caused by electron oscillations (plasmons) at the surface that are 'localized' within the nanostructure [25]. Various nanostructures such as nanoparticles, nanorods and other shapes have been studied for LSPR generation [25, 26]. LSPR is very sensitive to the refractive index of the surrounding medium [21] and this property can be harnessed for biomolecule or biomarker detection. Whenever there is a binding between the surface-bound ligands and free biomarkers or biomolecules on the plasmonic surface, there will be change in the refractive index (dielectric constant) of the surrounding medium. This change in refractive index contributes to a change in the resonant frequency of the plasmon and that phenomenon can be used for the detection of various biomarkers or biomolecules [27]. Various shapes, like lines, ledges, circles, rings, and squares, can be milled on the surface of nanostructured metal films [28]. Metal films with the subwavelength nanostructures [29] exhibit a phenomenon called extraordinary optical transmission (EOT) [20]; scientists make use of this property while fabricating various detection devices. The array of nanostructures milled over the metal surface in periodic fashion transmit more light than the bulk at certain wavelengths [30]. Transmission SPR spectroscopy (tSPR) based on EOT and LSPR [31, 32] is of interest to many researchers for sensing or detection devices. The tSPR can be used by measuring the EOT allowing for high transmission of light. The small size of these structures allows for easy incorporation of a light source and detector. This easy alignment and sensitivity due to EOT and LSPR allows for advancement in new lab on chip technology. This technology does not require any prisms, precision optics, or temperature control, further making tSPR-based sensors small, compact, and easy to carry [33]

In this work, detection of anti-insulin antibodies as a biomarker of type 1 diabetes (T1D) was chosen as a model system. Anti-insulin antibodies present in the body fight against the body's own insulin cells [34] and decrease the amount of insulin in the body which leads to insulin deficiency and results in T1D. The World Health Organization projects that the global prevalence of diabetes will increase from 217 million cases in 2005 to 366 million by 2030 [35]. Along with being a common disease in adults, diabetes is now the second most common pediatric disease. T1D is an autoimmune form of diabetes and the rate of T1D in children is rising with a 3% annual rate [36, 37]. Known for being a pediatric disease, T1D is now diagnosed during adulthood for approximately one quarter of patients [38]. T1D results from cellular mediated autoimmune destruction of the insulin producing pancreatic β-cells [39]. Patients suffering from T1D, frequently show life threating symptoms like ketoacidosis, and all

of them require insulin therapy for life. With the commencement or onset of T1D, patients have autoantibodies to at least one of the following: islet cell cytoplasm, insulin (insulin autoantibodies (IAAs)) [40], the 65-kDa isoform of glutamic acid decarboxylase (GAD65), insulinoma-associated antigen 2 (IA-2), and zinc transporter 8 (ZnT8) (these are collectively termed islet autoantibodies) [41, 42]. The development of T1D is predicted by islet autoantibodies. While both electrochemical and SPR methods have been developed for insulin assays [43], there is an unmet need of medical devices for quantification of islet autoantibodies. Current diabetes diagnostics tests like ELISA and lateral flow assay are slow and costly, thus making this key test less accessible in areas with limited resources. In spite of a need for better diagnostics tests, their development has been challenging. It has been demonstrated over the past two decades that usual platforms like lateral flow assays and ELISA do not perform up to the mark when applied to T1D diagnostics, and thus do not meet the sensitivity and specificity required for this medical situation [44, 45].

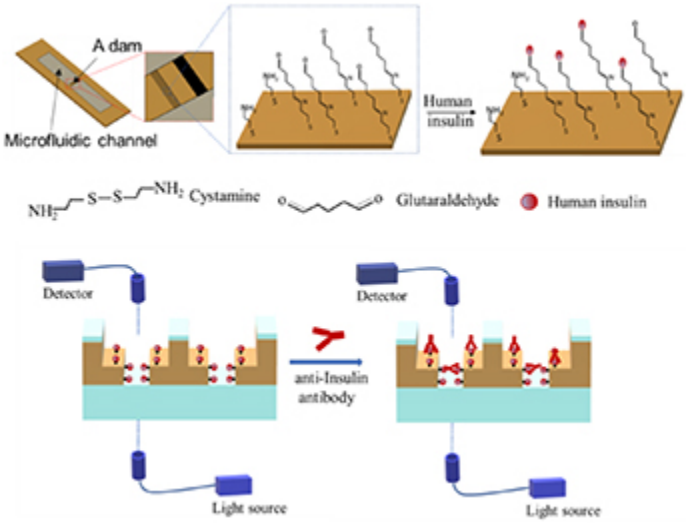


**Figure 1.** Illustration of the gold surface functionalization at the gold surfaces of the nanoledge array to immobilize human insulins and the model of plasmonic nanoledge device used for biomarker or biomolecule detection.

Based on recent advances in plasmonic nanoslit and nanoledge cavities for trapping and detection of various biomolecules or biomarkers [46], a plasmonic chip with a nanostructured nanoledge array in the metal film on a dam cross a microfluidic channel [46] was developed, as shown in figure 1, for the detection of anti-insulin antibodies of T1D. The dam structure crosses a micro-channel that offers an advantage of using less sample volume for analysis. The nanostructured ledge array fabricated on the dam provides better capture of small biomolecules/biomarkers than straight nanoslits as it combines 50 nm of inner slits and 280 nm of outer slit. Small biomolecules/biomarkers can be trapped inside the nanoledge slits and hence give better sample delivery and detection sensitivity. The fluidic dam was fabricated with lithography technique. Self-assembled monolayers (SAMs) were formed on the surface of the exposed gold in nanoledge array. This allowed for easy linkage of Human insulin to the gold surface. Then anti-insulin antibodies were flowed over the human insulin and monitored by a wavelength shift after binding between the anti-insulin antibodies and the human insulin platform. This overcomes the major challenges in rapid, sensitive, and specific diagnosis of T1D,

by allowing successful detection of ultra-low volumes of samples (buffer and human serum) containing T1D anti-insulin antibodies. This new platform offers promise to point-of-care detection of several isotypes of anti-insulin antibodies without any fluorescence labeling on a single chip [47].

## 2. Materials and experimental methods

### 2.1. Materials and reagents

Cystamine, glutaraldehyde, polyethylene glycol (PEG), human insulin and auto-insulin antibodies were purchased from Sigma-Aldrich and used without further purification. All other solvents and chemicals were purchased from Sigma-Aldrich. LS 1 light source was purchased from Ocean Optics.

### 2.2. Fabrication of nanoledge plasmonic chip

In this study, a lithography technique with focused ion beam (FIB) was developed, as shown in figure 2, to fabricate a flow-over fluidic dam with nanoledge structures. A multi-layer resist was used to get the side-wall sloped profile in the desired direction. Photomask was designed in Auto computer-aided design (Auto CAD) software. Glass substrates (Glove Scientific) were prepared by treatment with a piranha acid (3:1 $H_2SO_4$:$H_2O_2$) solution, rinsing with deionized (DI) water, and $N_2$ drying. The substrates were dehydrated on a hot plate for more than 5 min at temperature 90 °C. SU-8 3050 photoresist (MicroChem) was applied to a clean, dry glass slide. Subsequently, the substrate was soft-baked and flood-exposed (no mask) by OAI mask aligner (Milpitas, CA, USA) and then hard-baked to develop a structural layer of SU-8. A 100 nm $SiO_2$ film was then deposited by physical vapour deposition (PVD75, Kurt Lesker) upon the SU-8 layer. Subsequently, second layer of NFR 016 D2 negative photoresist (JSR Micro) was applied and patterned by standard photolithography technique. NFR 016 D2 was first spin applied and soft baked at 90 °C for 150 s on hot plate. Followed by exposure through the negative CAD photomask for 9 s by OAI mask aligner with the dose of 100 mJ $cm^{-2}$. Then the post bake was performed at 90 °C for 120 s, and resist was developed using PD523AD for 1 min, then rinsed with water, and dried with $N_2$ gun. Using the NFR resist as an etch mask, $CF_4$ and $O_2$ gases from a LAM Rainbow 4400 reactive ion etcher (RIE) were used to etch the oxide layer. The SU-8 layer was dry etched isotropically, in a controlled manner, with an $O_2$ plasma using $SiO_2$ as an etch mask. Etch parameters used were 100 mT pressure, RF power 100 W, bias −152 V, time 5 mins, $CF_4$ 45 sccm and $O_2$ 5 sccm flow rate. A small amount (about 3%–5%) of $SF_6$ was added to the gas mixture and it improved the surface roughness of the SU-8 layer. Regulating the etch chamber pressure, gas mixture, and RF power gave tunability to the slope and sidewall profile of the dam structures. Overcut sidewall profiles (slopes <90°) were desired and achieved by tuning the RIE's chamber parameters. The sloped profile with less than 90° angle can be easily coated uniformly everywhere by PVD. As PVD is a directional deposition technique, we need to have an overcut profile for uniform deposition of metal everywhere. The sloped profile was then transferred to PVD for deposition of 4 nm Ti + 250 nm Au + 4 nm Ti + 100 nm $SiO_2$, with the Ti layers serving as adhesion layers. The thicknesses of the film and the deposition rate were monitored with a quartz crystal microbalance (QCM) and were further checked with a profilometer (KLA Tencor P-10). Nanoledge structures were then milled into the

devices on top of the dam structures. Fibics software and a Zeiss Auriga Dual beam FIB/SEM were used for milling. Arrays of 100 nanoledge with 600 nm spacing periodicity between each structure were milled on the dam along with a reference box or burn box which did not have any gold film or any nanoledge structure. The 50 nm inner slit was milled using a 50-pA probe while the outer 280 nm step was milled using a 140-pA probe. We used 280 nm–50 nm dimensions as these dimensions have maximum plasmons generation efficiency based on previously reported results [48].

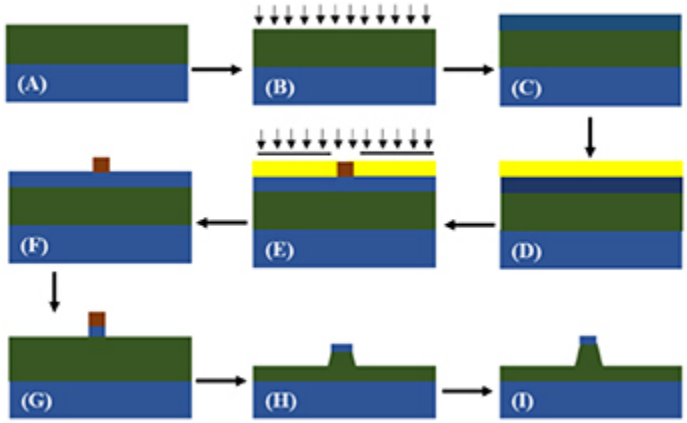


**Figure 2.** Fabrication process for the flow-over fluidic dam using a multi-layered resist (MLR) method. (A) Spin apply SU-8 photoresist and soft bake, (B) flood expose and bake the SU-8 post exposure, (C) deposit 100 nm of $SiO_2$ atop the cross-linked SU-8 structural layer, (D) spin apply JSR NFR 016D2 photoresist, (E) expose the JSR NFR photoresist through the photomask with design of the flow-over dam, (F) bake and develop the JSR NFR post exposure, (G) dry etch the $SiO_2$ layer with a $CF_4/O_2$ plasma, (H) dry etch the SU-8 layer with an $O_2$ plasma, (I) deposit 4 nm Ti, 250 nm Au, 4 nm Ti, and 100 nm $SiO_2$.

2.3. Functionalization of the plasmonic chip

Cystamine and glutaraldehyde chemistry were used to establish the self-assembled monolayer (SAM). A chip surface was thoroughly cleaned with an ethanol rinse, $O_2$ plasma clean, ethanol rinse, $N_2$ dry, and UV/ozone treatment. The oxygen plasma treatment was done for 5 min at 100 W in an oxygen plasma cleaner (South Bay Technologies PC-2000 Plasma Cleaner) at 178.6 mTorr $O_2$ pressure and a −783 volts DC bias. A 5 mm solution of cystamine in 90% ethanol solution was used to form a SAM with the reaction catalysis done by a microwave synthesizer. The disulfide bond within the cystamine molecule breaks and yields two sulfur-gold bonds at the surface of the chip. The substrate was then rinsed with an ethanol solution of 90% concentration and then rinsed with DI water in order to remove the unbound molecules. The terminal amine, sticking up from the surface, would then be able to bond to an aldehyde on the next reagent, glutaraldehyde, forming an imine bond. A 2.5% solution of glutaraldehyde was used to self-assemble atop of the formed cystamine layer. This provided a terminal aldehyde group to which human insulin can bind. A stock solution of 1 mg $ml^{-1}$ of anti-insulin antibody solution was diluted with a buffer and with human serum to yield a working solution of a different concentration. This solution was then delivered to the nanostructured plasmonic nanoledge area of the chip and allowed to bond for a few minutes. During this time the entire chip was encased in a high-humidity environment so that anti-insulin antibody solution would not dry up and

results in good binding between human insulin and anti-insulin antibodies. Afterwards, the chip was rinsed and dried with a $N_2$ stream. Then, the EOT measurements were taken with the modified microscopic spectroscopy.

The chips were re-usable. In order to regenerate the clean metallic surface, the adsorbed SAM could be removed by subjecting the substrates to oxygen plasma (South Bay Technologies, PC-2000 Plasma Cleaner) for 5 min at 100 W. The plasma treated substrates were then exposed to sonication in acetone, ethanol, then to water [49] and then were cleaned for 20 min by UV/ozone exposure [50] using a Bioforce UV/Ozone ProCleaner. It had previously been demonstrated that plasma cleaning does not adversely affect the metallic surfaces and does not add roughness to the surface [51]. This is in contrast to the roughness and pinholes that can occur by some cleaning methods, such as the use of piranha ($H_2SO_4$ and $H_2O_2$) [52].

## 3. Results and discussion

### 3.1. Fabrication results and optical characterization

SEM images of a typical fabricated plasmonic nanoledge device is shown in figure 3(a). Figure 3(b) shows the FIB images with good contrast which clearly shows the inner 50 nm nanoslit and outer 280 nm nanoslit. Each nanoledge has 280 nm outer width and 50 nm inner width slits with a periodicity of 600 nm. The 50 nm inner slits are to capture more biomolecules or biomarkers, thus increasing sensitivity and specificity.

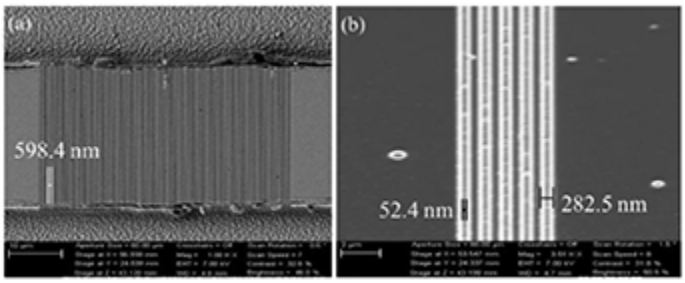


**Figure 3.** (a) SEM image ofnanoledge array with 600 nm of periodicity. (b) Represent the FIB images of the nanoledge.

Transmission spectrum measurements of plasmonic nanoledge chip were taken in air to gain the resonant peak locations. As shown in the optical transmission spectra in figure 4, the primary resonant peak locations are around 630–640 nm and 690–700 nm. Note that the transmission spectrum is the transmittance calculated after subtracting dark and reference. For the measurement, the light source was placed underneath the substrate and shone directly onto the underside of the dam, which contained the nanoledge structures without any modification. For nanoledge structures, which behave as 2D metallic nanomaterial, have two plasmon bands: longitudinal plasmons band (690–700 nm) and transverse plasmons (630–640 nm) [53]. The transverse plasmons are insensitive to size and surrounding medium but longitudinal plasmon band changes with the change in dielectric properties, size, shape and, refractive index of the surrounding medium [54]. This change of the peak or band with the change in surrounding medium is an indicator of sensor response. Here, the peak around 690–700 nm is due to longitudinal plasmons band and changes with the change in the refractive index of the

surrounding medium. The Gans theory explained the absorption spectra of the 2D metallic nanomaterials and shows how absorption spectra changes with the surrounding medium [55].

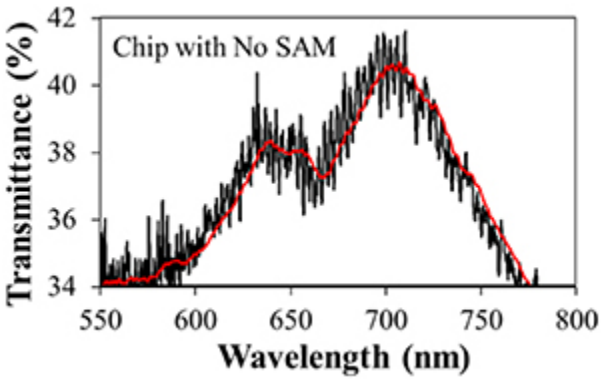


**Figure 4.** Represents the transmittance curve (smoothed in red color and, unsmoothed in black color) of fabricated plasmonic chip without any modification.

3.2. Optical detection of T1D biomarker

The anti-insulin antibody was used as a target in determining the sensitivity of the plasmonic nanoledge device fabricated and functionalized with different techniques, as shown in figure S1 (available online at stacks.iop.org/Nano/31/325503/mmedia), with the goal of determining if the device would be perceptive enough to determine the low concentration of anti-insulin antibodies in buffer and in human serum (HS). The plasmonic nanoledge device was functionalized with human insulin and then different concentrations of anti-insulin antibodies in buffer or human serum were flown over the functionalized device, and the optical transmission spectra were recorded using modified microscopic spectrometer (figures S2 and S4). Further, the recorded spectra were smoothed and fitted with the best fit polynomial function (up to 8th degree) for peak position determination. These experiments were performed with a microscopic spectrometer since it has a microscope and stage that allows for measurements to be taken only from the area of the device with the fabricated dam and nanoledge structures. For our transmission spectrum measurements, we used a broadband white light source (LS 1 Light source, 400–1100 nm) instead of typical lasers. The LS 1 light source was connected to the instrument with a fiber optic cable and light was shining on the back of the sample, allowing optical spectrum collection. The light transmittance of a sample at the detection nanoledge arrays was obtained by the equation below:

$$Transmittance = 100 \times \frac{slit - dark}{ref - dark}$$

where, *slit* represents the nanoledge array, *ref* is a burn box without any metal coating for full light transmission and, *dark* is any area coated with gold without any nanoledge or burn box and light is blocked.

To determine the peak wavelength shift in the transmission spectrum, a MATLAB program was created to fit the data using a certain order polynomial function to obtain smoothed transmittance curves. The transmittance spectra show red shift along with the antibody biomarker

concentration increase. A linear relationship between the concentration (Logarithm value) and wavelength shift was obtained (figure 6) which is typical for an affinity reaction-based sensing [56, 57]. Concentrations of 0.1, 1, 10, and 100 ng $ml^{-1}$ of anti-insulin antibody were used to demonstrate the detection capability of the plasmonic nanoledge device. The reaction time for each concentration was 15 mins and then the device was rinsed and dried with nitrogen stream. Then the three sets of the transmission spectra measured three times (3X3) for each concentration in buffer and in human serum, respectively, were recorded. For each concentration a total 9 measurements were taken. The results are summarized in tables S1 and S2.

Figures 5(a)–(b) show the normalized transmittance spectra of anti-insulin antibodies taken for different concentration in buffer and in human serum. The 100 ng $ml^{-1}$ shows the maximum shift and for 1 pg $ml^{-1}$ the shift is very small and almost insignificant. The peak shift was obtained by averaging the three sets of measurements. Figure 5(c)–(d) show the wavelength shift with respect to different concentrations of anti-insulin antibodies in buffer and in human serum, respectively. These plots both show high linearity, with correlation coefficient ($R^2$) above 0.97–0.98 for both buffer and human serum. The peak shift observed was due to the change in the refractive index at the surface of the plasmonic chip with the binding of anti-insulin antibodies. During the surface functionalization, the peak shift after each step of plasmonic chip functionalization was also recorded as shown in figure S3. In order to examine the background of human serum, human serum contains multiple proteins, but without added anti-insulin antibody, was performed and the results are shown in figure S5. The minimal plasmon peak shift during this control concludes that the specificity of human insulin functionalized plasmonic nanoledge chip is very high.

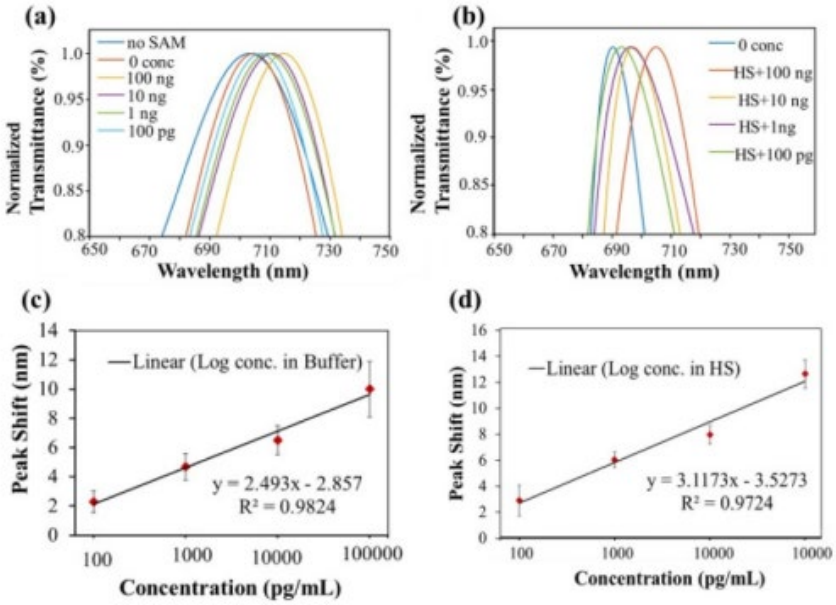


**Figure 5.** Representation of peak shift for anti-insulin antibody (a) in buffer and (b) in human serum; (c) and (d) show correlation of concentration of anti-insulin antibody with respect to wavelength peak shift, the straight line shows the linear fit.

3.3. Control experiments

Control experiments were performed to verify the specificity and selectivity of the human insulin modified plasmonic nanoledge device. Bovine serum albumin (BSA) and epidermal growth factor (EGF) of concentration (20 ng $ml^{-1}$) were used as a control. The optical peak shift of the insulin functionalized devices with flowing of BSA or EGF in the concentration (20 ng $ml^{-1}$) gives 0.1–0.2 nm from three trials (see table S3), indicating minimal non-specific binding of BSA and EGF to the human insulin-modified plasmonic nanoledge device. Three sets of individually functionalized devices for BSA and EGF binding were measured and the average peak shift is shown in figure 6.

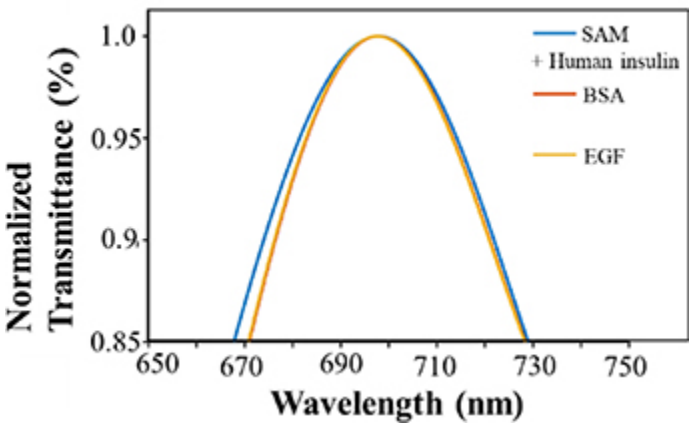


**Figure 6.** Measured peak shift for BSA and EGF to test the specificity of the plasmonic nanoledge device.

The measured results of the BSA and EGF interference are consistent and effective for the bioassay. The minimal non-specific binding of BSA and EGF to the detection devices indicates the high specificity of the designed biosensor. These results indicate that the plasmonic nanoledge device, along with tailored surface modification with appropriate receptors, can be used as biomarker or biomolecule detection with excellent sensitivity and specificity.

According to SPR sensing principle, there is a relationship between the wavelength shift and thickness of layer added as shown in equation (1) [46]:

$$\Delta\lambda = m(n_{\mathrm{A}} - n_{\mathrm{B}})[1 - \exp(-2d_{\mathrm{E}}/l_{\mathrm{d}})] \quad (1)$$

where $\Delta\lambda$ is the peak or wavelength shift, $m$is the refractive index unit (RIU) sensitivity, $n_{\mathrm{A}}$ and $n_{\mathrm{B}}$ are the refractive index of the medium at the plasmonic sensing surfaces in nanoledge arrays after and before the biological binding, $d_{\mathrm{E}}$ is the effective thickness of the added binding layer and, $l_{\mathrm{d}}$ is the decay length of surface plasmon mode. The addition of different concentrations of analytes into the plasmonic nanoledge device results in different layer thickness which changes the dielectric constant of the surrounding medium at the gold surfaces, eventually leading to peak shift. There is red shift with the greater concentration of the analytes because higher concentration means more binding and more peak shift. The peak shift as a function of the concentration obtained in this work is consistent with our previous results from both the theoretical simulation and experiments [46]. Advances in this work of using the plasmonic nanoledge device in human serum biomarker sensing further demonstrate a few advantages over other thin film based SPR devices in terms of sensitivity and specificity. The

device is $SiO_2$ coated at the top gold surfaces so it allows only in-cavity detection and avoids nonspecific binding at other surface [58]. The plasmonic nanoledge device with outer and inner width generates more coupled SPR-induced optical transmission and trap small size biomolecules or biomarkers to increase sensitivity [46]. This device has the potential application in the field of sensing and may be integrated with smart devices for point-of-care applications.

## 4. Conclusion

A novel plasmonic nanoledge device was fabricated with lithography and FIB technique, which has high sensitivity and selectivity. The plasmonic nanoledge device can be reused with simple cleaning in a plasma cleaner. The device can be used for biomolecule or biomarker detection by surface functionalization of the device accordingly. In this work, human insulin is used to modify the nanoledge devices and demonstrated for detection of anti-insulin antibody, a protein biomarker of T1D. The optical transmission peak shift was observed with the change in concentration of the protein biomarker binding reactions at the insulin functionalized device. The shift in peak wavelength is due to change in the refractive index or dielectric constant at the surface of the plasmonic nanoledge device. The sensitivity is high as it can detect in picograms concentration in buffer and in human serum. The background of human serum and additional control experiments using BSA and EGF indicate minimal interferences caused by non-specific binding to the insulin functionalized nanoledge arrays. This study offers promise for the development of a new planar plasmonic microfluidic LOC device for early and quick diagnosis of biomarkers in health care sectors.

## Acknowledgments

The authors acknowledge the financial support from U.S. NSF Grant No. (#1511194), NCBC technology enhancement Grant No. (#2019-TEG-1501), and NSF SBIR Grant No. (1913695). This work was performed at the Joint School of Nanoscience and Nanoengineering (JSNN), a member of Southeastern Nanotechnology Infrastructure Corridor (SENIC), and National Nanotechnology Coordinated Infrastructure (NNCI), which is supported by the National Science Foundation (ECCS-1542174).

Supplementary material for this article is available online at https://doi.org/10.1088/1361-6528/ab8c05.

## References

[1] Nimse S B, Sonawane M D, Song K-S and Kim T 2016 Biomarker detection technologies and future directions Analyst **141** 740–55 Crossref Google Scholar

[2] Li M, Cushing S K, Zhang J, Suri S, Evans R, Petros W P, Gibson L F, Ma D, Liu Y and Wu N 2013 Three-dimensional hierarchical plasmonic nano-architecture enhanced surface-enhanced raman scattering immunosensor for cancer biomarker detection in blood plasma ACS Nano **7** 4967–76 Crossref Google Scholar

[3] Donahue A C and Albitar M 2010 Recognition Receptors in Biosensors ed M Zourob (New York, NY: Springer) 221–48 Crossref Google Scholar

[4] Wang J, Wu L, Ren J and Qu X 2012 Visualizing human telomerase activity with primer-modified Au nanoparticles Small **8** 259–64 Crossref Google Scholar

[5] Labib M, Khan N, Ghobadloo S M, Cheng J, Pezacki J P and Berezovski M V 2013 Three-mode electrochemical sensing of ultralow microRNA levels J. Am. Chem. Soc. **135** 3027–38 Crossref Google Scholar

[6] Krishnamoorthy S 2015 Nanostructured sensors for biomedical applications—a current perspective Curr. Opin. Biotechnol. **34** 118–24 Crossref Google Scholar

[7] Homola J and Piliarik M 2006 Surface Plasmon Resonance Based Sensors (Berlin: Springer) 45–67 Crossref Google Scholar

[8] Prabowo B A, Purwidyantri A and Liu K-C 2018 Surface plasmon resonance optical sensor: a review on light source technology Biosensors **8** 80 Crossref Google Scholar

[9] Seiler S T, Rich I S and Lindquist N C 2016 Direct spectral imaging of plasmonic nanohole arrays for real-time sensing Nanotechnology **27** 184001 IOPscience Google Scholar

[10] Zhu J, Wang Z, Lin S, Jiang S, Liu X and Guo S 2020 Low-cost flexible plasmonic nanobump metasurfaces for label-free sensing of serum tumor marker Biosens. Bioelectron. **150** 111905 Crossref Google Scholar

[11] Zeng Y et al 2017 Recent advances in surface plasmon resonance imaging: detection speed, sensitivity, and portability Nanophotonics **6** 1017–30 Crossref Google Scholar

[12] Zhou J, Tao F, Zhu J, Lin S, Wang Z, Wang X, Ou J-Y, Li Y and Liu Qing H 2019 Portable tumor biosensing of serum by plasmonic biochips in combination with nanoimprint and microfluidics Nanophotonics **8** 307–16 Crossref Google Scholar

[13] Olaru A, Bala C, Jaffrezic-Renault N and Aboul-Enein H Y 2015 Surface plasmon resonance (SPR) biosensors in pharmaceutical analysis Crit. Rev. Anal. Chem. **45** 97–105 Crossref Google Scholar

[14] Masson J-F 2017 Surface plasmon resonance clinical biosensors for medical diagnostics ACS Sens. **2** 16–30 Crossref Google Scholar

[15] Hill R T 2015 Plasmonic biosensors WIREs Nanomed. Nanobiotechnol. **7** 152–68 Crossref Google Scholar

[16] Firdous S, Anwar S and Rafya R 2018 Development of surface plasmon resonance (SPR) biosensors for use in the diagnostics of malignant and infectious diseases Laser Phys. Lett. **15** 065602 IOPscience Google Scholar

[17] Zhu J, Chen X, Xie Y, Ou J-Y, Chen H and Liu Qing H 2020 Imprinted plasmonic measuring nanocylinders for nanoscale volumes of materials Nanophotonics 167–76 Crossref Google Scholar

[18] Jung W, Han J, Choi J-W and Ahn C H 2015 Point-of-care testing (POCT) diagnostic systems using microfluidic lab-on-a-chip technologies Microelectron. Eng. **132** 46–57 Crossref Google Scholar

[19] Xia M, Zhang P, Qiao K, Bai Y and Xie Y-H 2016 Coupling SPP with LSPR for enhanced field confinement: a simulation study J. Phys. Chem. C **120** 527–33 Crossref Google Scholar

[20] Ebbesen T W, Lezec H J, Ghaemi H F, Thio T and Wolff P A 1998 Extraordinary optical transmission through sub-wavelength hole arrays Nature **391** 667–9 Crossref Google Scholar

[21] Mayer K M and Hafner J H 2011 Localized surface plasmon resonance sensors Chem. Rev. **111** 3828–57 Crossref Google Scholar

[22] Bagra B, Zhang W, Zeng Z, Mabe T and Wei J 2019 Plasmon-enhanced fluorescence of carbon nanodots in gold nanoslit cavities Langmuir **35** 8903–9 Crossref Google Scholar

[23] Mabe T, Zeng Z, Bagra B, Ryan J and Wei J 2018 Surface plasmon resonance of a bimetallic nanostructured film for enhanced optical sensitivity ChemistrySelect **3** 3018–23 Crossref Google Scholar

[24] Zeng Z, Mabe T, Zhang W, Bagra B, Ji Z, Yin Z, Allado K and Wei J 2018 Plasmon–exciton coupling in photosystem I based biohybrid photoelectrochemical cells ACS Appl. Bio Mater. **1** 802–7 Crossref Google Scholar

[25] Willets K A and Duyne R P V 2007 Localized surface plasmon resonance spectroscopy and sensing Annu. Rev. Phys. Chem. **58** 267–97 Crossref Google Scholar

[26] Gupta B D and Kant R 2018 [INVITED] Recent advances in surface plasmon resonance based fiber optic chemical and biosensors utilizing bulk and nanostructures Opt. Laser Technol. **101** 144–61 Crossref Google Scholar

[27] Akimoto T, Sasaki S, Ikebukuro K and Karube I 1999 Refractive-index and thickness sensitivity in surface plasmon resonance spectroscopy Appl. Opt. **38** 4058–64 Crossref Google Scholar

[28] Singh P 2016 SPR biosensors: historical perspectives and current challenges Sens. Actuator B: Chem. **229** 110–30 Crossref Google Scholar

[29] Barnes W L, Dereux A and Ebbesen T W 2003 Surface plasmon subwavelength optics Nature **424** 824–30 Crossref Google Scholar

[30] Gay G, Alloschery O, Viaris de Lesegno B, O'Dwyer C, Weiner J and Lezec H J 2006 The optical response of nanostructured surfaces and the composite diffracted evanescent wave model Nat. Phys. **2** 262 Crossref Google Scholar

[31] Yue W, Wang Z, Yang Y, Li J, Wu Y, Chen L, Ooi B, Wang X and Zhang X-X 2014 Enhanced extraordinary optical transmission (EOT) through arrays of bridged nanohole pairs and their sensing applications Nanoscale **6** 7917–23 Crossref Google Scholar

[32] Tu L, Huang L and Wang W 2019 A novel micromachined Fabry-Perot interferometer integrating nano-holes and dielectrophoresis for enhanced biochemical sensing Biosens. Bioelectron. **127** 19–24 Crossref Google Scholar

[33] Wang M, Zhao C, Miao X, Zhao Y, Rufo J, Liu Y J, Huang T J and Zheng Y 2015 Plasmofluidics: merging light and fluids at the micro-/nanoscale Small **11** 4423–44 Crossref Google Scholar

[34] Pihoker C, Gilliam L K, Hampe C S and Lernmark Å 2005 Autoantibodies in diabetes Diabetes **54** S52–S61 Crossref Google Scholar

[35] Smyth S and Heron A 2006 Diabetes and obesity: the twin epidemics Nat. Med. **12** 75 Crossref Google Scholar

[36] 2007 Chapter one: diabetes in children: epidemiology Pediatr. Diabetes **8** 10–8 Crossref Google Scholar

[37] Karvonen M, Viik-Kajander M, Moltchanova E, Libman I, LaPorte R and Tuomilehto J 2000 Incidence of childhood type 1 diabetes worldwide. Diabetes Mondiale (DiaMond) project group Diabetes Care **23** 1516–26 Crossref Google Scholar

[38] Maahs D M, West N A, Lawrence J M and Mayer-Davis E J 2010 Epidemiology of type 1 diabetes Endocri. Metab. Clin. **39** 481–97 Crossref Google Scholar

[39] Atkinson M A, Eisenbarth G S and Michels A W 2014 Type 1 diabetes Lancet **383** 69–82 Crossref Google Scholar

[40] Ziegler A G et al 2013 Seroconversion to multiple islet autoantibodies and risk of progression to diabetes in children JAMA **309** 2473–9 Crossref Google Scholar

[41] Sacks D B and Kricka L J 2015 Plasmonic chip tackles type 1 diabetes diagnosis Clin. Chem. **61** 794–6 Crossref Google Scholar

[42] Zhang B, Kumar R B, Dai H and Feldman B J 2014 A plasmonic chip for biomarker discovery and diagnosis of type 1 diabetes Nat. Med. **20** 948 Crossref Google Scholar

[43] Singh V and Krishnan S 2018 Electrochemical and surface plasmon insulin assays on clinical samples Analyst **143** 1544–55 Crossref Google Scholar

[44] Greenbaum C J, Palmer J P, Kuglin B and Kolb H 1992 Insulin autoantibodies measured by radioimmunoassay methodology are more related to insulin-dependent diabetes mellitus than those measured by enzyme-linked immunosorbent assay: results of the fourth international workshop on the standardization of insulin autoantibody measurement J. Clin. Endocrinol. Metab. **74** 1040–4 Google Scholar

[45] Liu E and Eisenbarth G S 2007 Accepting clocks that tell time poorly: fluid phase versus standard ELISA autoantibody assays Clin. Immunol. **125** 120–6 Crossref Google Scholar

[46] Zeng Z, Shi X, Mabe T, Christie S, Gilmore G, Smith A W and Wei J 2017 Protein trapping in plasmonic nanoslit and nanoledge cavities: the behavior and sensing Anal. Chem. **89** 5221–9 Crossref Google Scholar

[47] Pandey C M, Augustine S, Kumar S, Kumar S, Nara S, Srivastava S and Malhotra B D 2018 Microfluidics based point-of-care diagnostics Biotechnol. J. **13** 1700047 Crossref Google Scholar

[48] Zeng Z, Mendis M N, Waldeck D H and Wei J 2016 A semi-analytical decomposition analysis of surface plasmon generation and the optimal nanoledge plasmonic device RSC Adv. **6** 17196–203 Crossref Google Scholar

[49] Benesch J, Mano J F and Reis R L 2010 Analysing protein competition on self-assembled mono-layers studied with quartz crystal microbalance Acta Biomater. **6** 3499–505 Crossref Google Scholar

[50] Ron H, Matlis S and Rubinstein I 1998 Self-assembled monolayers on oxidized metals. 2. Gold surface oxidative pretreatment, monolayer properties, and depression formation Langmuir **14** 1116–21 Crossref Google Scholar

[51] Berman D and Krim J 2012 Impact of oxygen and argon plasma exposure on the roughness of gold film surfaces Thin Solid Films **520** 6201–6 Crossref Google Scholar

[52] Kang J and Rowntree P A 2007 Gold film surface preparation for self-assembled monolayer studies Langmuir **23** 509–16 Crossref Google Scholar

[53] Cao J, Sun T and Grattan K T V 2014 Gold nanorod-based localized surface plasmon resonance biosensors: a review Sens. Actuator B: Chem. **195** 332–51 Crossref Google Scholar

[54] Huang X, Neretina S and El-Sayed M A 2009 Gold nanorods: from synthesis and properties to biological and biomedical applications Adv. Mater. **21** 4880–910 Crossref Google Scholar

[55] Link S, Mohamed M B and El-Sayed M A 1999 Simulation of the optical absorption spectra of gold nanorods as a function of their aspect ratio and the effect of the medium dielectric constant J. Phys. Chem. B **103** 3073–7 Crossref Google Scholar

[56] Li Z, Zhang H, Ge X, Liang Y, An X, Yang C, Fang B, Xie H and Wei J 2013 A nanocomposite of copper(ii) functionalized graphene and application for sensing sulfurated organophosphorus pesticides New J. Chem. **37** 3956–63 Crossref Google Scholar

[57] Sanders M, Lin Y, Wei J, Bono T and Lindquist R G 2014 An enhanced LSPR fiber-optic nanoprobe for ultrasensitive detection of protein biomarkers Biosens. Bioelectron. **61** 95–101 Crossref Google Scholar

[58] Lee K-L, Wang W-S and Wei P-K 2008 Sensitive label-free biosensors by using gap plasmons in gold nanoslits Biosens. Bioelectron. **24** 210–5 Crossref Google Scholar